Int. J. Heat Mass Transfer. Vol. 12, pp. 1627–1639. Pergamon Press 1969. Printed in Great Britain

THE INITIAL VAPOR BUBBLE GROWTH ON A HEATED WALL DURING NUCLEATE BOILING

V. SERNAS* and F. C. HOOPER†

(*Received* 5 *April* 1968 *and in revised form* 9 *April* 1969)

Abstract—An experimental investigation of the initial vapor bubble growth on a horizontal, heated wall during saturated pool boiling is reported. Streak photography has been adapted for the first time to the observation of bubble growth rates. When combined with high-speed framing photography this has proven to be an effective technique for the observation of the initial growth of a bubble because the uncertainty in the zero time datum can be reduced to about 10μs. This compares with a correspondingly uncertainty of at least 100μs in previously reported works which used high-speed framing photography alone.

Hemispherical bubbles were measured during the first 500μs following nucleation. The growth curves showed the liquid momentum effects were not significant beyond the first 50μs. For the time period between 50 and 500μs following nucleation, the data fitted very closely the one half power, $R = mt^{\frac{1}{2}}$, where R is the bubble radius, m the growth constant and t the time.

The measured growth constant was compared with those predicted from five different analytical models, and was found to correspond closely to a model which postulated a "thick" microlayer of constant thickness underlying the bubble. "Thick" implied a sufficient thickness to delay the arrival of the temperature wave at the microlayer liquid–heated-surface interface until some time later than 500μs.

NOMENCLATURE

A, area;
c, specific heat (constant pressure);
h_{fg}, latent heat of vaporization;
k, thermal conductivity;
l, microlayer thickness;
m, vapor bubble growth constant defined by $R = mt^{\frac{1}{2}}$;
p, pressure;
q, heat rate;
q/A, heat flux density;
r, radial distance co-ordinate in spherical co-ordinates;
R, radius of bubble;
$\dot{R}$, $\frac{dR}{dt}$, velocity of vapor–liquid interface;
t, time;
T, temperature;
T_{sat}, liquid saturation temperature;
T_{sup}, superheat temperature;
ΔT_{sat}, $T_{sup} - T_{sat}$;
x, distance co-ordinate perpendicular to heater surface;
Y, $(k_l^2/k_s^2 l^2)\,\alpha_s t$;
α, thermal diffusivity;
γ, $= \dfrac{k_s \rho_s c_s}{k_l \rho_l c_l}$;
Δ, signifying a difference;
ρ, density;
Ψ, dimensionless radius used in Fig. 6.

Subscripts

l, pertaining to the liquid;
s, pertaining to the solid;
v, pertaining to the vapor;
w, pertaining to the wall.

* Assistant Professor of Mechanical and Aerospace Engineering, Rutgers University, New Brunswick, New Jersey.

† Professor of Mechanical Engineering, University of Toronto, Toronto, Canada.

INTRODUCTION

HIGH-SPEED photography techniques have been used by many investigators [1–5 and others] in explorations of the mechanism of nucleate boiling heat transfer. Experimental difficulties have usually limited the range of each investigation to a particular phase of a vapor bubble's growth. This investigation was similarly restricted, being concerned with the observation of vapor bubble growth rates very close to the time of nucleation. No experiments have previously been reported for this time region, which has been labelled in the literature as the initial growth period. To make observations in this period it was necessary to attain framing speeds much higher than those previously used, and ultimately to introduce a new streak photography technique in order to observe bubble growth closer to the time of nucleation than the highest available framing speed of 14000 frames/s would allow.

EXPERIMENTAL EQUIPMENT

The boiling experiments were carried out in a stainless steel, aquarium-type tank, 8 in. long, 5 in. wide and 5 in. high. The two larger sides of the tank had glass windows, and the two smaller sides supported nickel plated, 300 W, immersion heaters, shaped to provide distributed heating and to maintain the water in the tank at saturation temperature. The tank was vented to the atmosphere. Isolated vapor bubbles were generated on an electrically heated, horizontal, Chromel C ribbon, $\frac{1}{16}$ in. wide, $1\frac{1}{2}$ in. long and 0·0031 in. thick. A copper–constantan thermocouple made from 0·0031 in. thermocouple wire was capacitor-discharge welded in an argon atmosphere to the bottom surface of the heated strip. A coating of clear epoxy cement was then applied to the undersurface of the strip. The Chromel C strip was held under slight tension between two horizontal brass rods that conveyed the dici heating curren from 1 6V battery. The position of the Chromel C strip could be translated in all three perpendicular directions, and also rotated about its own longitudinal centerline, by adjustments made from outside of the tank itself.

The heating strip width of $\frac{1}{16}$ in. was a compromise between a wide ribbon or plate, that would better approximate an infinite horizontal boiling surface, and a wire that could be sharply focused in profile on the film. A wide heating ribbon would refract the light rays traveling through the thermal boundary layer to such an extent that a small bubble on the surface would not be visible at all. Furthermore, a wide ribbon

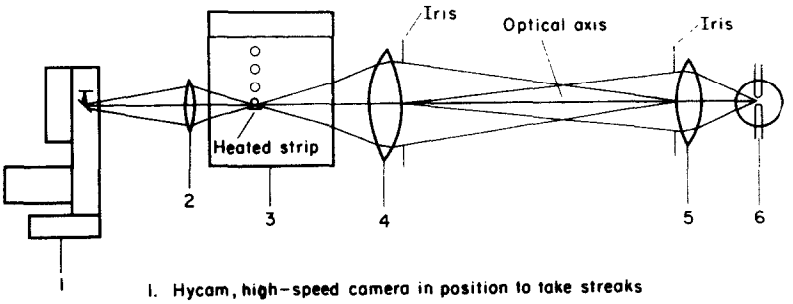

1. Hycam, high-speed camera in position to take streaks
2. Microscope objective lens, f = 48mm
3. Boiling water tank
4. Microscope condenser lens, f = 203mm
5. Lamp condenser lens, f = 130mm
6. Mercury arc lamp, 250W

FIG. 1. Schematic diagram of experimental equipment.

could produce a number of natural nucleation sites in the line of observation and render the study of isolated bubbles impractical. A profile view of a bubble growing on a natural site on a wire is difficult to obtain because one cannot determine if the nucleating cavity is exactly on the tangential line of sight. A width of $\frac{1}{16}$ in. was chosen because it was found that the refraction caused by this width was sufficiently small to permit the surface to be focused reasonably sharply.

The boiling water tank was mounted on a 16 ft long optical bench that contained a high intensity illumination system and a high speed camera (see Fig. 1). A high intensity mercury arc was focused through the two lenses comprising the Koehler illumination system to produce a circular area of illumination, controllable in size and intensity, which backlighted the growing bubble on the heated Chromel C strip. This illumination system provided sufficient light to obtain a profile bubble photograph, enlarged about six times on the Tri-X reversal film, with an exposure time of about 3 μs. The Hycam high-speed motion picture camera was also equipped with a streak photography attachment that allowed streak traces to be made of bubbles nucleating at the same source at which bubbles had been recorded on a framing basis a short time before. A more detailed description of the apparatus can be obtained from [6].

EXPERIMENTAL PROCEDURE

Distilled water was boiled in the tank for at least four hours before any testing was begun. The heated strip was then energized for at least an hour to degas the cavities in the strip. It was noted that artificial cavities made by a phonograph diamond needle were initially the only active sites, but ceased to be active after about 10 min. The current in the heated strip was then increased and these cavities again became active along with some other natural sites. The artificial cavities however failed to nucleate after a time and left only natural sites active. The heat flux was then adjusted to give only 1 or 2 active sites on the strip. A few strips were discarded as useless at this stage since they produced active sites that were too close to one another. A site was named suitable when it was within half a strip width of a thermocouple and did not have other active sites near it.

The whole boiling tank was then moved on its traversing table to bring the chosen nucleating site on to the optical axis of the Koehler illumination system. The strip was rotated about its longitudinal axis until the profile position was located. The camera was loaded with 16 mm Tri-X film and the microscope was adjusted to focus a sharp image of the heated strip on the film before triggering the camera.

The procedure for taking a streak film varied only in the preparation of the camera. Since it was necessary to invert the film for taking the streak traces, time marks were put on the streak film by a flashing stroboscope illuminating the streak knife-edges every 2·5 ms with a short light pulse which appeared as a bar across the developed film (see Fig. 3).

ZERO TIME DATUM

The difficulty in obtaining the time at which a bubble starts to grow on a high-speed framing film has been pointed out in the literature [1]. One frame may show no bubble while the next frame may show a bubble that is already quite large in size. The recorded bubble must actually have begun to grow at some time in the interval between the taking of the two frames; therefore, the location of zero time on a framing film can be determined only within the time interval between two frames. For example, at a framing speed of 2500 frames/s, two frames are separated by a time interval of 400 μs, or at 14000 frames/s by 70 μs.

A much more precise method of obtaining the zero time datum is by streak photography. In this technique, the bubble image is focused on a thin slit formed by a pair of adjustable knife-edges. The film moving at a high speed immediately behind the slit which spans the film is

exposed by the light coming through the slit. If a nucleation site is perfectly centered on the slit, the image of a growing bubble begins to block light from one end of the slit immediately upon the formation of the bubble and progressively obscures the light across the width of the film as the bubble grows. For a film speed of about 150 ft/s, the location of time zero on the film can be determined to within 3 microseconds for a centered image, and within an estimated 10 microseconds for a slightly off-centered image. Radius or velocity measurements from the streak are uncertain at these small times because of the inherent blur, but one can definitely observe that a small bubble of poorly defined radius does exist there, and thus one can pin-point zero time to within the above stated limits on the streak trace. It would require a framing camera faster than 100000 frames/s to locate zero time within the same limits.

RESULTS

Growth rate of hemispherical bubbles

Of all the bubble growth sequences photographed in this study the ones that lend themselves most readily to analytical treatment are the hemispherical bubbles of Films 20 and 21 shown in Figs. 2 and 3 respectively. The average heater temperature was 23°F above the water saturation temperature while these two films were being taken. The fact that the bubbles on Fig. 2 are hemispherical can be easily verified by means of a compass. It is not immediately obvious, however, that the streaks of Fig. 3 are traces of hemispherical bubbles slightly misaligned with the streak slit. Four arguments were found to show that the streaks of Fig. 3 were those of hemispherical bubbles:

1. The waiting times of the bubbles recorded by these streaks were about 100 ms, a period similar to those found for the hemispherical bubbles of Fig. 2. Other sequences in this study have shown that the waiting times for oblate bubbles were about 10 ms, and for spherical bubbles about 1 ms. Johnson, de la Pena and Mesler [7] have also found that the waiting time is a function of the shape of the bubble.

2. The bubbles of Figs. 2 and 3 were taken only a few minutes apart at the same nucleating site. This site differed from the sites that produced spherical and oblate bubbles.

3. The plots of radius vs. time of the streaks of Fig. 3 showed almost the same growth rates as found for the hemispherical bubbles of Fig. 2.

4. Every bubble recorded in this study showed a bright spot of light within it. This bright spot is the location where the light rays from behind the bubble passed directly through the bubble. It can serve as an excellent indicator of the shape of the bubble because at that location in the bubble the liquid–vapor interfaces must be approximately perpendicular to the optical axis. Some of the streak traces of Fig. 3 recorded this bright spot starting some six frame lengths from the beginning of the bubble streak. Since this bright streak trace was located near the heater wall, the bubbles must have been hemispherical at that time. The fact that the traces of the bright spot did not start at the same location as the traces of the bubble implies that the

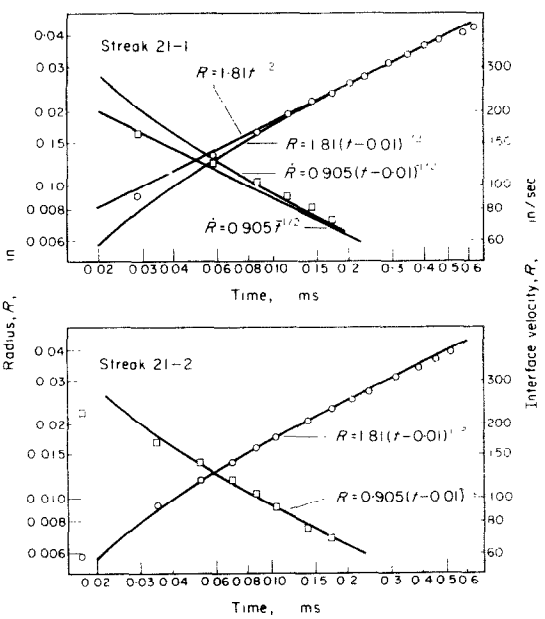

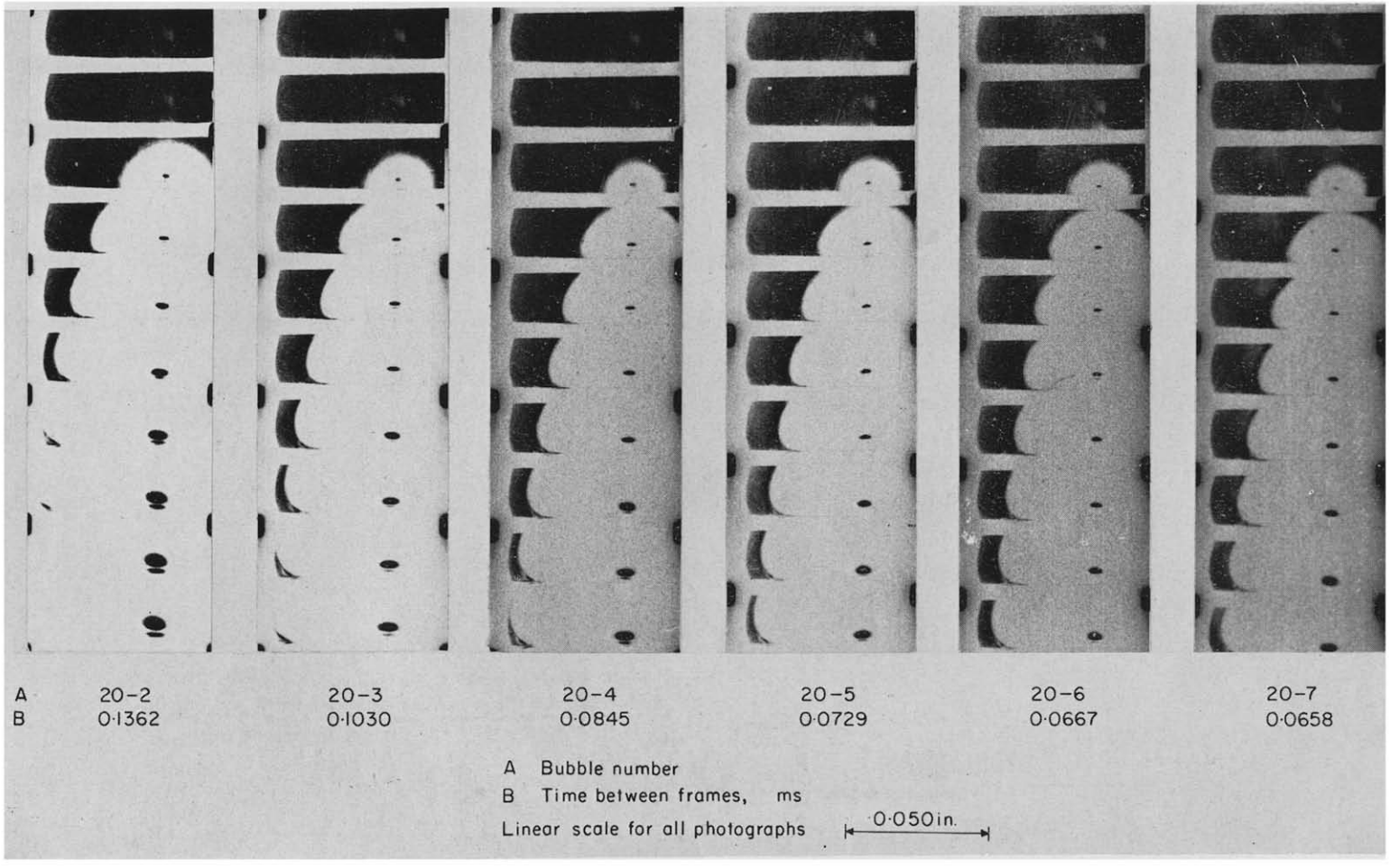

FIG. 2. Six hemispherical bubble beginnings from Film 20.

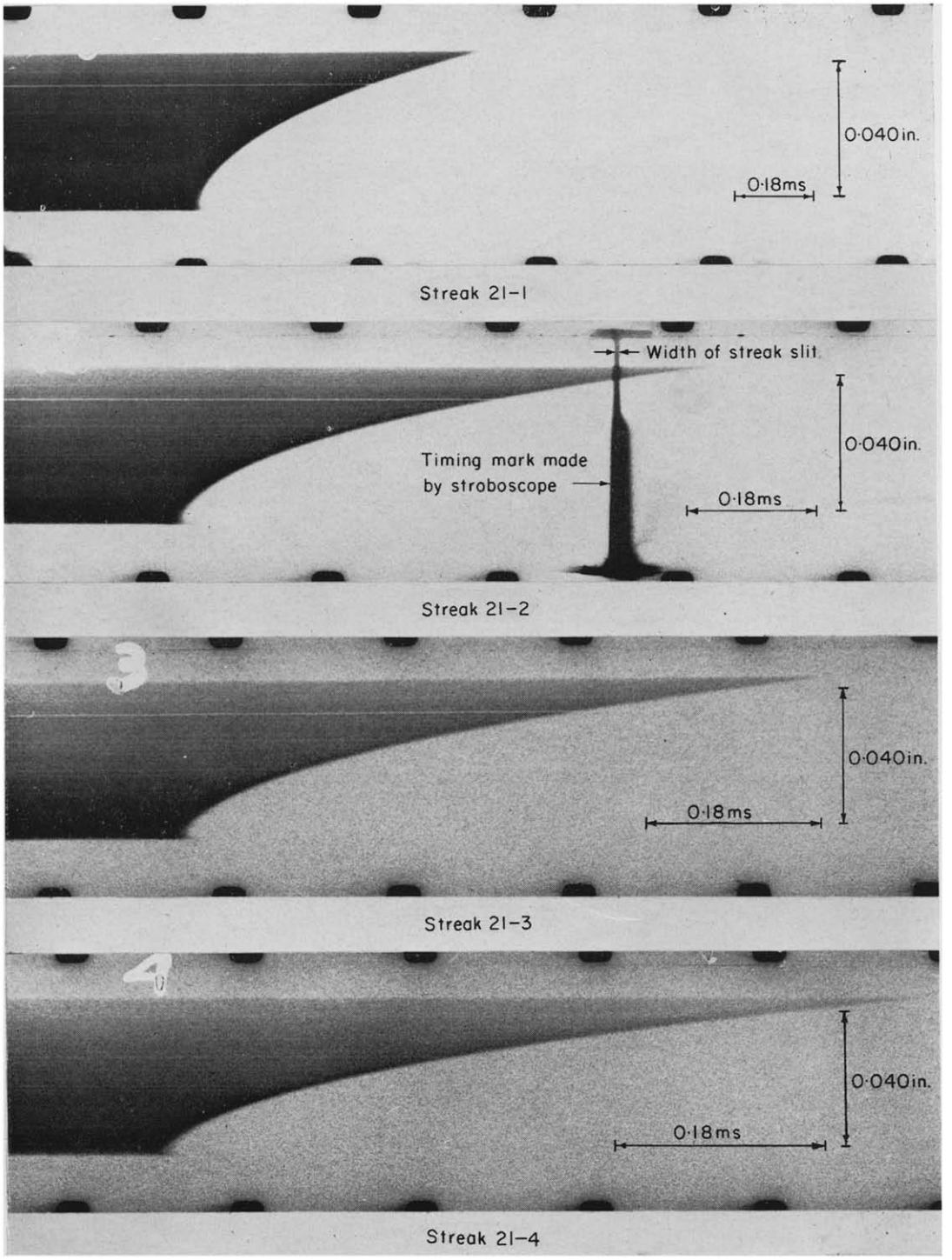

FIG. 3. Four streaks of hemispherical bubble beginnings from Film 21.

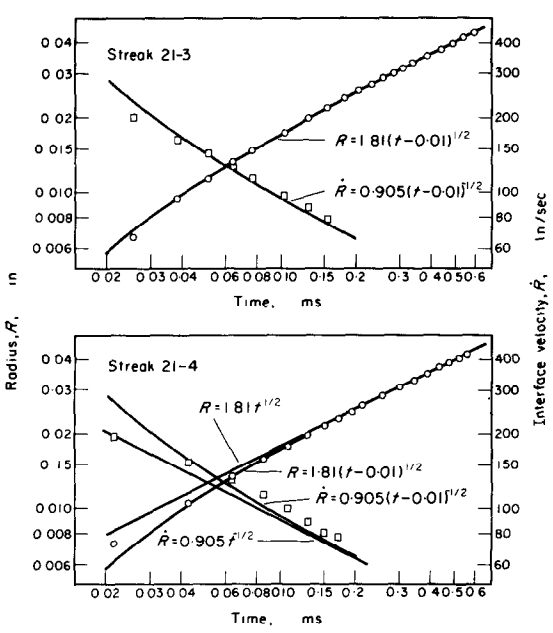

FIG. 4. Bubble radius and velocity vs. time for bubbles of Film 21. The zero time datum on these plots was estimated from the streak traces and can be in error by 0·01 ms. The solid lines are plots of the indicated mathematical equations and are not necessarily the best fit lines.

bubble image was somewhat misaligned with the streak slit.

It can be seen from the results plotted on Fig. 4 that except for the very beginning, the hemispherical bubbles grew in a manner that could be described, in the interval $0 < t < 0{\cdot}5$ ms, by the equation $R = 1{\cdot}81\ t^{\frac{1}{2}}$. The growth constant for the remaining nine hemispherical bubbles shown in Figs. 2 and 3 but not given in Fig. 4, varied from 1·68 to 1·95 in/s$^{\frac{1}{2}}$. The growth of *spherical* bubbles in uniformly superheated liquids is also proportional to $t^{\frac{1}{2}}$ and it is governed by transient heat conduction into the vapor bubble. Scriven [8] obtained for the growth of a spherical bubble the expression

$$R = 2\sqrt{\frac{3}{\pi}\frac{\Delta T_{\text{sat}}}{\rho_v h_{fg}}}\sqrt{(k_l\rho_l c_l)}\ t^{\frac{1}{2}}. \qquad (1)$$

This yields $R = 1{\cdot}27\ t^{\frac{1}{2}}$ for 23°F superheated water. It is clear that the experimental results yield a growth rate much faster than that predicted by equation (1). It was observed from many framed sequences that only the hemispherical bubbles had such a high growth rate, and that the oblate and spherical bubbles grew much more slowly at the same heater wall temperature.

The primary difference between a hemispherical and an oblate bubble is the area of contact with the heater. Spherical bubbles have very little contact with the heated wall and oblate bubbles tend to attain a fixed area of contact and then not to expand along the heater surface as the volume of the bubble increases further. A hemispherical bubble, however, has a heater contact area that is at all times about one half the area of contact between the vapor and the bulk liquid.

It has been established [9–11] that a very thin microlayer of liquid is left on the heater surface as a vapor bubble expands while in contact with the heater surface. Therefore it is expected that a hemispherical bubble would have a film on the surface at its base that is about one half the area of contact of the bulk liquid with the vapor. The vaporization of this film can be expected to contribute a substantial amount of vapor to the volume of a growing hemispherical bubble. Several analytical models, incorporating a microlayer of constant thickness, were examined to see if the predicted growth of the radius could be of the form $R = mt^{\frac{1}{2}}$ and if the resultant growth constant, m, compared well with the experimentally observed value of 1·81 in/s$^{\frac{1}{2}}$. For simplicity, it was assumed that the liquid was uniformly superheated to the temperature of the heater. In reality, however, a temperature gradient must have existed in the liquid. The thickness of the temperature boundary layer was probably much thicker than the one measured by Marcus and Dropkin [12] since there were no other bubbles produced on the Chromel C heating strip except for those recorded on the film. Five analytical models of a growing hemispherical bubble follow. It must of course be recognized that these are certainly not the only models that may be postulated; however,

it is felt that they incorporate most of the alternative assumptions which can be considered realistic on physical grounds for a microlayer of constant thickness.

(a) *Adiabatic wall.* If it is assumed that the base of the hemispherical bubble does *not* contribute any heat to the bubble, and that all the heat comes from the bulk superheated liquid through the hemispherical liquid–vapor interface, the growth of the hemispherical bubble would be the same as that given by equation (1), i.e. $R = 1{\cdot}27\, t^{\frac{1}{2}}$.

The approximate temperature profiles within the liquid and the solid for this and the following cases are given in Fig. 5.

(b) *Very thin isothermal microlayer at* T_{sat}. If it is assumed that the microlayer is continuous but very thin, initially at T_{sup}, and that its temperature drops to T_{sat} throughout its depth immediately upon formation, the microlayer is assigned no thermal capacity and an infinite conductivity. The surface of the heater under the bubble, initially at T_{sup}, would then reach T_{sat} immediately upon the formation of the thin microlayer above it. The solid would thus conduct a significant amount of heat to the bubble and affect the growth rate of the bubble. Letting the growth of the hemispherical bubble be $R = mt^{\frac{1}{2}}$, one can solve for m using the above mentioned simplified physical model of the microlayer.

From the solution for the spherical bubble, i.e. equation (1), it is known that the instantaneous total heat flux through the hemispherical vapor–liquid interface at time t is

$$q_l = \sqrt{3}\frac{k_l \Delta T_{sat}}{(\pi \alpha_l t)^{\frac{1}{2}}}(2\pi R^2) = \sqrt{3}\frac{k_l \Delta T_{sat}}{(\pi\alpha_l)^{\frac{1}{2}}}\frac{R}{m}(2\pi R^2)$$
$$= 2(3\pi)^{\frac{1}{2}}\, m(k_l \rho_l c_l)^{\frac{1}{2}} \Delta T_{sat} R. \qquad (2)$$

The instantaneous heat flux density from the solid is a function of the distance from the center of the bubble i.e. the nucleating site. At a distance

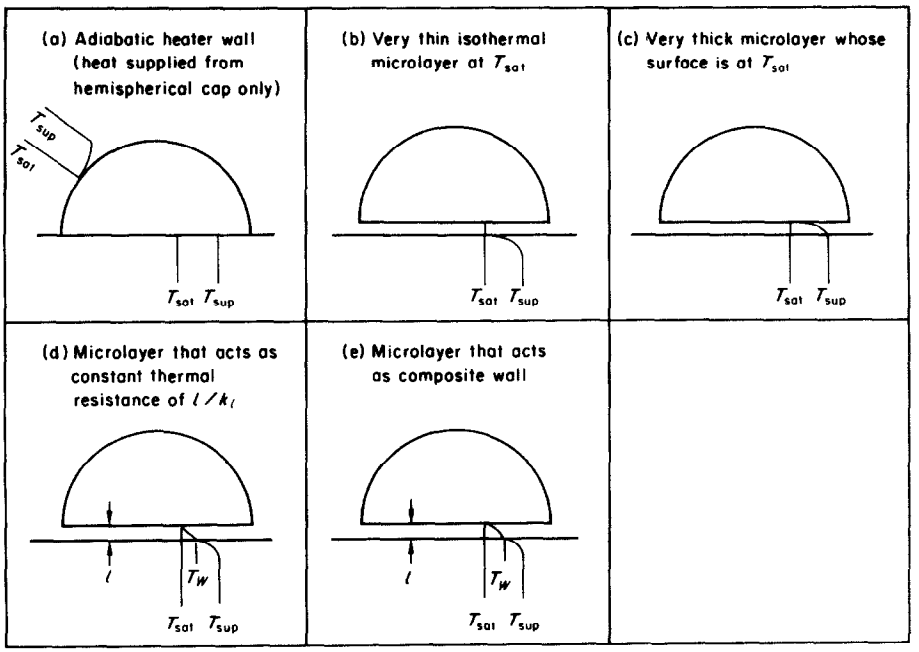

FIG. 5. Summary of the temperature profiles through the microlayer and the underlying solid due to various assumptions about the microlayer at $t < 0{\cdot}5$ ms. The profiles are diagrammatic and not necessarily to scale.

$r (r < R)$ from the center, the surface has been exposed to T_{sat} for a time equal to $(R/m)^2 - (r/m)^2$. Assuming one dimensional heat conduction from a semi-infinite solid, one obtains the instantaneous heat flux density through the flat base at position r as

$$\frac{q_s}{A} = \frac{k_s \Delta T_{sat}}{(\pi \alpha_s)^{\frac{1}{2}} (1/m) (R^2 - r^2)^{\frac{1}{2}}}.$$

The instantaneous total heat flux coming from the circular base of the bubble at time t is then

$$q_s = 2\pi \int_{r=0}^{R} \frac{q_s}{A} \, r \, dr$$

$$= \frac{2\pi k_s \Delta T_{sat}}{(\pi \alpha_s)^{\frac{1}{2}} 1/m} \int_{r=0}^{R} \frac{r \, dr}{(R^2 - r^2)^{\frac{1}{2}}}$$

$$= 2\pi^{\frac{1}{2}} m (k_s \rho_s c_s)^{\frac{1}{2}} \Delta T_{sat} R. \quad (3)$$

Combining equations (2) and (3) into a heat balance, one gets

$$\rho_v h_{fg} \frac{dV}{dt} = \rho_v h_{fg} 2\pi R^2 \frac{m^2}{2R}$$

$$= 2(3\pi)^{\frac{1}{2}} m (k_l \rho_l c_l)^{\frac{1}{2}} \Delta T_{sat} R + 2\pi^{\frac{1}{2}} m (k_s \rho_s c_s)^{\frac{1}{2}} \Delta T_{sat} R. \quad (4)$$

Solving for m, one gets

$$m = 2 \sqrt{\frac{3}{\pi} \frac{\Delta T_{sat}}{\rho_v h_{fg}}} \left[(k_l \rho_l c_l)^{\frac{1}{2}} + \frac{1}{\sqrt{3}} (k_s \rho_s c_s)^{\frac{1}{2}} \right]. \quad (4a)$$

Comparing equation (4a) with equation (1) gives one the difference between an adiabatic wall boundary condition and a heat conducting wall. It should be remembered that liquid must be present on the wall surface in order to absorb as latent heat the heat conducted from the wall as implied by the heat balance of equation (4).

Substitution of numerical values corresponding to the test conditions into equation (4a) with $\Delta T_{sat} = 23°F$, yields $m = 4{\cdot}16$ in/s$^{\frac{1}{2}}$.

(c) *Very thick microlayer.* If it is assumed that the microlayer's vapor–liquid interface temperature drops from T_{sup} to T_{sat} immediately upon the formation of the microlayer, and that the temperature wave through the microlayer does not reach the underlying solid in the time interval $0 < t < 0{\cdot}5$ ms, the bubble base can be taken as a semi-infinite slab of water conducting heat into the bubble at the vapor–liquid interface following the initial stepwise temperature drop of ΔT_{sat} at the time of formation of the microlayer.

The instantaneous total heat flux through the vapor–liquid interface is again expressed by equation (2), and the instantaneous total heat flux coming from the base is expressed by equation (3) with only the term $(k_s \rho_s c_s)^{\frac{1}{2}}$ replaced by $(k_l \rho_l c_l)^{\frac{1}{2}}$. Using a heat balance of the form of equation (4), one can solve for the value of m, as

$$m = 2 \sqrt{\frac{3}{\pi} \frac{\Delta T_{sat}}{\rho_v h_{fg}}} (k_l \rho_l c_l)^{\frac{1}{2}} \left(1 + \frac{1}{\sqrt{3}} \right). \quad (5)$$

Substitution of numerical values corresponding to the test conditions into equation (5) with $\Delta T_{sat} = 23°F$, yields $m = 1{\cdot}90$ in/s$^{\frac{1}{2}}$.

(d) *Microlayer that acts as a thermal resistance, constant at l/k_l.* It has been suggested by Cooper and Lloyd [13] that the microlayer may act as a thin layer of relatively high thermal resistance between the heat supplying wall and the vapor interface of the bubble. Neglecting the heat capacity of the thin microlayer, and assuming that the liquid–vapor interface of the microlayer suddenly drops to T_{sat} upon the formation of the microlayer, and that this surface remains at T_{sat} for $t > 0$, one can write the heat flux density from the bubble base as

$$\frac{q_s}{A} = \frac{k_l}{l} (T_w - T_{sat}), \quad (6)$$

where l is the microlayer thickness. The surface temperature of the wall is obtained from the well known expression—e.g. p. 71 of Carslaw and Jaeger [14].

$$\frac{T_w - T_{sat}}{\Delta T_{sat}} = \exp\left(\frac{k_l^2 \alpha_s t}{k_s^2 l^2}\right) \operatorname{erfc}\left\{\frac{k_l}{k_s l}(\alpha_s t)^{\frac{1}{2}}\right\}. \quad (7)$$

Substituting equation (7) into equation (6), and integrating over the bubble base area, one gets an expression for the instantaneous total heat being transferred at time t from the bubble base, i.e.

$$q_s = \frac{k_l \Delta T_{sat}}{l} 2\pi \int_{r=0}^{R} \exp\left(\frac{k_l^2 \alpha_s}{k_s^2 l^2} \frac{R^2 - r^2}{m^2}\right) \operatorname{erfc}\left\{\left[\frac{k_l^2}{k_s^2 l^2} \alpha_s \frac{(R^2 - r^2)}{m^2}\right]^{\frac{1}{2}}\right\} r \, dr. \quad (8)$$

Letting

$$\frac{k_l^2 \alpha_s}{k_s^2 l^2}\left(\frac{R^2 - r^2}{m^2}\right) = y = \frac{k_l^2 \alpha_s t}{k_s^2 l^2}$$

and rearranging equation (8), one gets

$$\left(\frac{l}{k_l}\right) \frac{k_l^2}{k_s^2 l^2} \frac{\alpha_s}{\pi m^2} \frac{q_s}{\Delta T_{sat}} = \int_0^y e^y \operatorname{erfc} y^{\frac{1}{2}} dy. \quad (9)$$

The instantaneous total heat flux through the hemispherical vapor–liquid interface at time t can be obtained from equation (2). Multiplying both sides of equation (2) by

$$\left(\frac{l}{k_l}\right) \frac{k_l^2}{k_s^2 l^2} \frac{\alpha_s}{\pi m^2},$$

and letting

$$\gamma = \left[\frac{k_s \rho_s c_s}{k_l \rho_l c_l}\right]^{\frac{1}{2}},$$

one gets

$$\left(\frac{l}{k_l}\right) \frac{k_l^2}{k_s^2 l^2} \frac{\alpha_s}{\pi m^2} \frac{q_l}{\Delta T_{sat}} = 2\sqrt{\frac{3}{\pi}} \frac{1}{\gamma} y^{\frac{1}{2}}. \quad (10)$$

Equations (9) and (10) are nondimensional expressions for the instantaneous heat flux into the bubble from the base and the hemispherical cap respectively. Since it is the instantaneous heat flux that determines the instantaneous bubble growth rate, a nondimensional expression can be obtained for the bubble radius by making a heat balance of the form

$$q_s + q_l = h_{fg} \rho_v \frac{dV}{dt} = h_{fg} \rho_v \pi m^2 R,$$

which can be rearranged to yield

$$\frac{l}{k_l} \frac{k_l^2}{k_s^2 l^2} \frac{\alpha_s}{\pi m^2} (q_s + q_l) = \left(\frac{k_l}{l}\right)\left(\frac{\alpha_s}{k_s^2}\right)\left(\frac{\rho_v h_{fg}}{\Delta T_{sat}}\right) R = \int_0^y e^y \operatorname{erfc} y^{\frac{1}{2}} dy + 2\sqrt{\frac{3}{\pi}} \frac{1}{\gamma} y^{\frac{1}{2}}. \quad (11)$$

This nondimensional expression for the radius has been plotted on Fig. 6. The abscissa of Fig. 6 was chosen as $\sqrt{y}$ instead of y, because the relationship $R = mt^{\frac{1}{2}}$ plots as a straight line through the origin in these co-ordinates. It can readily be seen from the inset of Fig. 6 that the heat flux from the bubble base under the assumptions of case (*d*) is not proportional to $t^{\frac{1}{2}}$ at any time t. Therefore, the assumption that heat is transferred through a constant thickness microlayer according to equation (6) at $t < 0{\cdot}5$ ms is rejected.

(e) *Composite wall.* Consider the microlayer to be of constant thickness, l, initially at T_{sup}, and to have constant thermal properties ρ_l, c_l, k_l and α_l. Assume that this microlayer lies on a semi-infinite block of Chromel C, initially at T_{sup}, and that the liquid–vapor interface of the microlayer drops to T_{sat} immediately upon the formation of the microlayer. These assumptions constitute the problem of a film, the thermal capacity of which is taken into consideration, overlying a solid with different thermal properties, under the boundary condition

$$k_l \frac{dT_l}{dx} = k_s \frac{dT_s}{dx}$$

at the film–solid interface. The heat flux density across the liquid–vapor interface has been derived by Carslaw and Jaeger [14] p. 322 as:

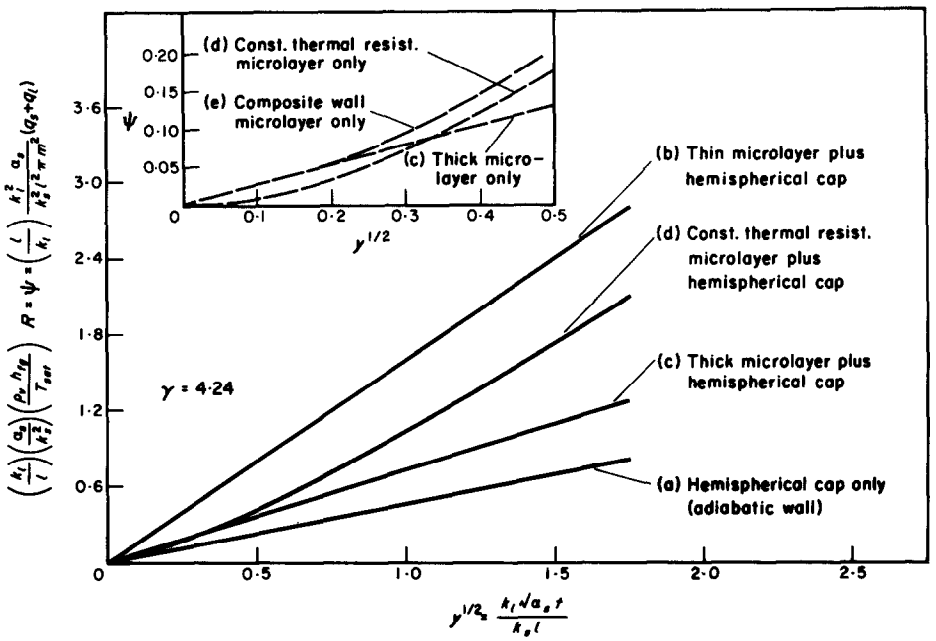

FIG. 6. Comparison of the instantaneous total heat supplied to a hemispherical vapor bubble for various assumptions about the microlayer. Since the ordinate is also a dimensionless radius, the solid lines are plots of bubble growth equations.

$$\frac{q_s}{A} = \frac{\Delta T_{sat} k_l}{\sqrt{(\pi \alpha_l)}} \times$$

$$\left\{1 + 2 \sum_{n=1}^{\infty} \left(\frac{\gamma - 1}{\gamma + 1}\right)^n \exp\left(-n^2 l^2 / \alpha_l t\right)\right\}. \qquad (12)$$

For thick microlayers or short times, the exponentials can be approximated by zero, and the heat flux density from the microlayer is the same as that without any thermal influence from the underlying solid, i.e. case (c):

$$\frac{q_s}{A} = \frac{\Delta T_{sat} k_l}{(\pi \alpha_l t)^{\frac{1}{2}}}.$$

For very thin microlayers or large times, the exponentials can be replaced by unity. The heat flux density from the microlayer then becomes the same as in case (b), i.e.

$$\frac{q_s}{A} = \frac{\Delta T_{sat} k_l}{(\pi \alpha_l t)^{\frac{1}{2}}} \left[\frac{k_s \rho_s c_s}{k_l \rho_l c_l}\right]^{\frac{1}{2}} = \frac{T_{sat} k_s}{(\pi \alpha_s t)^{\frac{1}{2}}}.$$

After a nondimensionalizing procedure, similar to that described in detail in case (d), instantaneous total heat supplied to the bubble from the composite wall microlayer has been worked out and plotted in the inset of Fig. 6. It can be seen from the inset of Fig. 6 that for $(k_l/k_s l)(\alpha_s t)^{\frac{1}{2}} < 0{\cdot}2$ no appreciable difference exists in the total instantaneous heat supplied by a thick microlayer and a composite wall microlayer.

In summing up the five cases, it can be seen that only three cases yield a growth of the form $R = mt^{\frac{1}{2}}$ i.e.

(1) the adiabatic wall case for which the growth constant is 1·27 in/s$^{\frac{1}{2}}$.

(2) the "thick" microlayer case for which the growth constant is 1·90 in/s$^{\frac{1}{2}}$, and

(3) the thin isothermal microlayer case for which the growth constant is 4·16 in/s$^{\frac{1}{2}}$.

The measured value of 1·81 for the growth constant is very close to the calculated value

for the "thick" microlayer case and quite distant from the other two cases. It is concluded, therefore, that a simple "thick" microlayer model adequately describes the growth rate of a hemispherical bubble in the interval $0 < t < 0{\cdot}5$ ms.

Liquid momentum influence

The four streak traces of Fig. 3 were carefully re-examined to determine when the radius of the hemispherical bubbles began to follow the equation $R = mt^{\frac{1}{2}}$. From each of the four streak traces the radius and the liquid–vapor interface velocity were measured at equal small increments of time and then plotted on a linear scale against time. Figure 7 shows the result obtained from streak 21–2. Plots of equations of the form $R = mt^{\frac{1}{2}}$ and $\dot{R} = (m/2)\,t^{-\frac{1}{2}}$ were then made on transparent paper and superimposed upon the graphs containing the data points. By sliding the two pages relative to each other a position was found at which most data points for the radius coincided with the algebraic equation, $R = mt^{\frac{1}{2}}$. However, at that position the zero time data of the two superimposed graphs did not match, and also the first few velocity points did not fall on the curve, $\dot{R} = (m/2)\,t^{-\frac{1}{2}}$. A deviation of the velocity for a short length of time from the minus one half power law does not measurably change the radius. Therefore, it is not surprising that the radius data points fit the $\frac{1}{2}$ power law while the velocity showed some deviation at the beginning. The point in time at which both the velocity points and the radius points begin to coincide with their respective power equations was found to be about 40–50 μs from the time zero datum established from the streak trace. However, this time datum can be in error from 3 to 10 μs due to optical misalignment. Therefore, the estimated initial growth period from nucleation to the time at which the growth begins to follow the law $R = mt^{\frac{1}{2}}$ is from 43 to 60 μs, with 50 μs as the most probable time.

Theoretical analysis of the initial growth rate of spherical bubbles [15, 16] has indicated that the growth rate of spherical bubbles is initially controlled by liquid momentum and subsequently by transient heat conduction. Direct experimental verification of their theoretical results is not available in the literature. No similar theoretical analysis exists for vapor bubbles growing on the surface of a heated solid, but it can be seen that transient heat conduction.

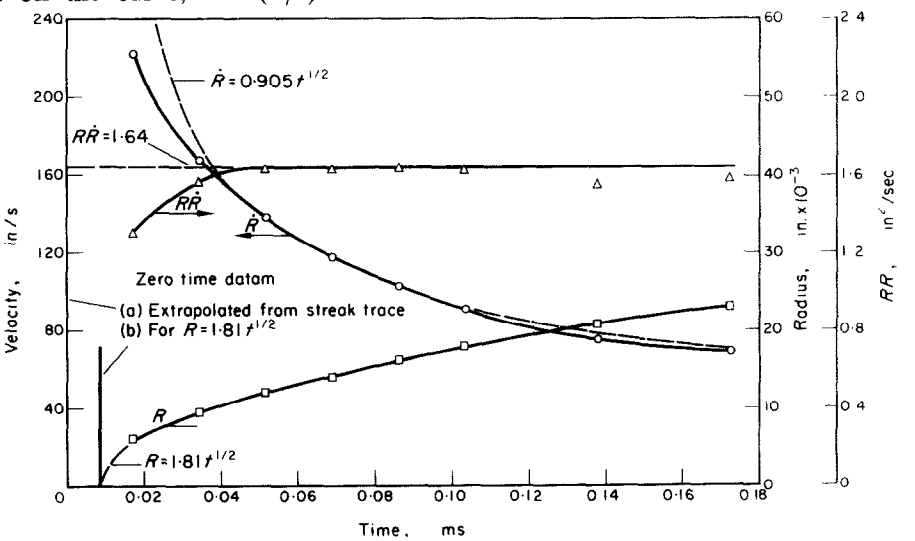

FIG. 7. Comparison of the radius and velocity measurements from streak 21–2 with the equations $R = 1{\cdot}81\,t^{\frac{1}{2}}$ and $R = 0{\cdot}905\,t^{-\frac{1}{2}}$.

resulting in a growth of $R = mt^{\frac{1}{2}}$, takes over at about 50 μ s from nucleation for the bubbles observed in Film 21. It can be inferred, therefore, that in the interval from zero to 50 μs the liquid momentum significantly influences the growth of a hemispherical bubble on a heated wall.

The extraction of the liquid momentum influence interval could only be accomplished from the streak traces such as those of Fig. 3, and could not have been made from the data obtained from framing sequences such as those in Fig. 2. The reasons for this are threefold:

1. The zero time datum of the framing sequences can be determined with available equipment only to within some 70 μ s, a time interval greater than the one that is being measured.

2. The instantaneous velocity of the liquid–vapor interface cannot be measured from such framing sequences. In the initial growth interval it is the velocity that is perceptively different from the minus one half power law.

3. An insufficient number of data points is available close to nucleation, i.e. a framing speed of 14000 frames/s is too slow to detect any deviation from $R = mt^{\frac{1}{2}}$ in the first 50 μs.

Framing speeds of 14000 frames/s would have been sufficient to determine that the hemispherical bubbles followed a $\frac{1}{2}$ power law for most of the 500 μs interval following nucleation. As a matter of fact, the plots of radius vs. time obtained from the framing sequences of Fig. 2 showed such a dependence very nicely.

CONCLUSIONS

The following conclusions can be made from the results of this study:

1. Streak photography, combined with high-speed framing photography, can yield more information about the initial vapor bubble growth than high-speed framing photography alone.

2. The growth of a hemispherical vapor bubble in atmospheric, saturated water is significantly influenced by the liquid momentum only for the first 50 μ s following nucleation.

3. In the interval between 50–500 μ s after nucleation the radius of hemispherical vapor bubbles growing on a heated wall whose average temperature was 23°F above the saturated temperature of the liquid water increased, on the average, according to the equation $R = 1{\cdot}81\ t^{\frac{1}{2}}$. A simple model incorporating a superheated microlayer of constant thickness adequately describes this growth behavior.

REFERENCES

1. P. H. STRENGE, A. ORELL and J. W. WESTWATER, Microscopic study of bubble growth during necleate boiling, *A.I.Ch.E. Jl* **7**, 578 (1961).
2. J. M. YATABE and J. W. WESTWATER, Bubble growth rates for ethanol–water and ethanol–isopropanol mixtures, Preprint 7, Eighth National Heat Transfer Conference, Los Angeles (1965).
3. R. F. GARTNER, Photographic study of nucleate pool boiling on a horizontal surface, *J. Heat Transfer* **87**, 17 (1965).
4. J. R. HOWELL and R. SIEGEL, Incipience, growth and detachment of boiling bubbles in saturated water from artificial nucleation sites of known geometry and size, *Proc. 3rd Int. Heat Transfer Conf.*, Chicago (1966).
5. A. P. HATTON and I. S. HALL, Photographic study of boiling on prepared surfaces, *Proc. 3rd Int. Heat Transfer Conf.*, Chicago (1966).
6. V. SERNAS, Initial vapor bubble growth on a heated wall during nucleate boiling, Ph.D. Thesis, University of Toronto (1967).
7. M. A. JOHNSON JR., J. DE LA PENA and R. B. MESLER, Bubble shapes in nucleate boiling, *Chem. Engng Prog. Symp.* **62**, 1 (1966).
8. L. E. SCRIVEN, On the dynamics of phase growth, *Chem. Engng Sci.* **10**, 1 (1959).
9. F. D. MOORE and R. B. MESLER, The measurement of rapid surface temperature fluctuations during nucleate boiling of water, *A.I.Ch.E. Jl* **7**, 620 (1961).
10. R. R. SHARP, The nature of liquid film evaporation during nucleate boiling, NASA TN D-1997 (1964).
11. R. C. HENDRICKS and R. R. SHARP, Initiation of cooling due to bubble growth on a heated surface, NASA TN D-2290 (1964).
12. B. D. MARCUS and D. DROPKIN, Measured temperature profiles within the superheated boundary layer above a horizontal surface in saturated nucleate pool boiling of water, *J. Heat Transfer*, **87**, 333 (1965).
13. M. G. COOPER and A. J. P. LLOYD, Transient local heat flux in nucleate boiling, *Proc. 3rd Int. Heat Transfer Conf.*, Chicago (1966).
14. H. S. CARSLAW and J. C. JAEGER, *Conduction of Heat in Solids*, 2nd edn. Oxford University Press (1959).

15. S. A. ZWICK and M. S. PLESSET, On the dynamics of small vapour bubbles in liquids, *J. Math. Phys.* **33**, 308 (1955).

16. H. K. FOSTER and N. ZUBER, Growth of a vapor bubble in a superheated liquid, *J. Appl. Phys.* **25**, 474 (1954).

Résumé—On décrit une étude expérimentale de la croissance initiale des bulles de vapeur sur une paroi chauffée horizontale pendant l'ébullition, saturée on réservoir. La photographie à fente a été adaptée pour la première fois à l'observation des vitesses de croissance de bulles. Cela s'est montré, lorsqu'on la combine avec la photographie ultra-rapide, être une technique efficace pour l'observation de la croissance initiale d'une bulle parce que l'incertitude dans l'origine des temps peut être réduite à 10 μs Ceci peut être comparé avec une incertitude correspondante d'au moins 100 μs dans les travaux publiés auparavant qui utilisaient seulement la photographie ultrarapide.

Des bulles hémisphériques ont été mesurées pendant les 500 premières μs suivant la nucléation. Les courbes de croissance ont montré que les effets de quantité de mouvement du liquide n'étaient pas importants après les 50 premières μs. Pour la période de temps entre 50 et 500 μs après la nucléation, les résultats se plaçaient très près de la loi en puissance un demi, $R = mt^{\frac{1}{2}}$, où R est le rayon de la bulle, m la constante de croissance, et t le temps.

La constante de croissance mesurée a été comparée avec celles prédites à partir de cinq modèles analytiques différents, et correspond de près à un modèle qui supposait une microcouche "épaisse" d'épaisseur constante à la base de la bulle. L'adjectif "épais" implique une épaisseur suffisante pour retarder l'arrivée de l'onde de température à l'interface entre la microcouche liquide et la surface chauffée pendant un temps quelque peu supérieur à 500 μs.

Zusammenfassung—Es wird über eine experimentelle Untersuchung des beginnenden Blasenwachstums an einer horizontalen Heizfläche bei gesättigtem Behältersieden berichtet. Zum erstenmal wurde Schlierenphotographie zur Beobachtung der Blasenwachstumsraten angewandt. Kombiniert mit Hochgeschwindigkeitsfilmaufnahmen erwies sich dies als wirkungsvolle Methode für die Beobachtung des beginnenden Wachstums einer Blase, da die Unsicherheit für den Initialzeitpunkt auf etwa 10 Microsekungen reduziert werden kann; dies im Vergleich zu einer entsprechenden Unsicherheit von wenigstens 100 Microsekunden in früheren Arbeiten, in denen Hochgeschwindigkeitsphotographie allein verwendet wurde.

Während der ersten 500 Microsekunden nach der Keimbildung wurden halbkreisförmige Blasen vermessen. Die Wachstumskurve zeigte, dass die Flüssigkeitskräfte über die ersten 50 Microsekunden hinaus nicht wesentlich waren. In der Zeitspanne zwischen 50 und 500 Microsekunden nach der Keimbildung folgten die Werte sehr genau der Wurzelbeziehung $R = mt^{\frac{1}{2}}$, wobei R der Blasenradius ist, m die Wachstumskonstante und t die Zeit.

Die gemessene Wachstumskonstante wurde mit der nach fünf verschiedenen analytischen Modellen vorherbestimmten Konstanten verglichen, und es zeigte sich eine genaue Übereinstimmung mit einem Modell, das eine "dicke" Mikrogrenzschicht konstanter Dicke unterhalb der Blase forderte.

"Dick" bedeutet eine genügende Dicke, um die Ankunft der Temperaturwelle an der der Heizfläche zugewandten Seite der Mikroschicht auf eine Zeit von etwas über 500 Microsekunden zu verzögern.

Аннотация—Излагается экспериментальное исследование начального роста пузырьков пара на горизонтальной нагретой стенке при насыщенном кипении в большом объеме. Для наблюдения за скоростью роста пузырьков впервые применялось шлиренфотография. В сочетании со скоростной киносъемкой она представляет эффективное средство для наблюдения за начальным ростом пузырьков, т.к. неопределенность начала отсчета времени может быть снижена до 10 микросекунд. Этот результат можно сравнить с начальной неопределенностью, равной по крайней мере 100 микросекундам, полученной в предыдущих работах, с использованием только скоростной киносъемки.

В первые 500 микросекунд после начала образования пузырьков наблюдались полусферические пузырьки. Кривые роста, показывающие влияние количества движения жидкости, не были характерными по истечении первых 50 микросекунд. За время от 50 до 500 микросекунд после момента начала образования пузырьков данные очень близко соответствуют $\frac{1}{2}$ в выражении $R = mt^{\frac{1}{2}}$, где R — радиус пузырька, m — постоянная роста, а t — время. Измеренная константа роста сравнивалась с расчетами по пяти

различным моделям. Нашли, что она соответствует модели, которая постулирует «толстый» микрослой постоянной толщины под пузырьком, что означает толщину, достаточную для того, чтобы замедлить прибытие температурной волны на микрослой поверхности раздела жидкость-нагретая поверхность более чем на 500 микросекунд.